Chapter 3

Model Definition

This model was designed to take into account the change in strength and ductility of concrete due to confinement. Ductility is a measure of the failure strain relative to the yield or peak strain. Previous researchers have utilized two different approaches when modeling these effects. The "effective confinement" approach [(Mander et al., 1988b), (Ahmad and Shah, 1982), (Sheikh and Uzumeri, 1982)] estimates the amount of confining pressure that the confinement applies on the concrete. This is typically done by estimating the stress in the confining material, the effectiveness of the confinement over the cross section, and other cross sectional properties. It is assumed that this confining pressure will be constant throughout the loading. The increase in concrete strength is then determined by considering experimental results of concrete at an equivalent confining pressure. Therefore, any change in the concrete behavior due to a change in the confinement pressure cannot be captured with this method. The "effective confinement" method cannot explicitly include the variation in the stress throughout the cross section or the change in confinement pressure with loading or changing confinement material properties. The second approach, which was chosen for this thesis, is to implicitly model the effect of concrete confinement by including it in the concrete plasticity theory. In this method, the confinement mechanism is modeled explicitly in the finite element (FE) model. By explicitly including the confining material, this method allows any form of confinement (active or passive) and any confining material (for example, rebar, steel jackets, or fiber reinforced polymer (FRP) sheets) to be modeled. Interaction between the concrete and the confining

mechanism is properly accounted for. For example, fracture of a stirrup in a column, and the subsequent drastic change in the confinement level of the concrete, leading to a change in the behavior of the concrete itself, can be modeled. Even the effect of the variable confinement over the cross section of a tied column can be modeled.

The ability to accurately represent the three-dimensional behavior of concrete is fundamental to the approach taken in this thesis. Once the failure surface is reached, the current three-dimensional load state of the concrete directly affects the failure surface location and rate of damage accumulation. Through this approach, confinement can come not only from the traditional forms of rebar or FRP jackets, but also from loading in perpendicular directions. By understanding and modeling the actual three-dimensional behavior of the concrete under true triaxial loading conditions, the model is more flexible than the "effective confinement" models. It can be applied to more diverse structures instead of being limited to simple columns with designated types of confinement.

It is not the intention that all aspects of concrete behavior be included in the model defined in this thesis. Creep, fracture, shear sliding, strain rate effects, and cyclic loading behaviors are not built into the present model. Tension strength is also not included. The specimen is assumed to be pre-cracked, thus the initial tension strength is set to zero. At a later date, this model could be incorporated into an existing framework that includes these behaviors [for example, ABAQUS ABAQUS (Inc.) or ADINA ADINA R&D (Inc.)] to create a complete, versatile concrete model. However, the scope of this thesis is limited to monotonic compression or bending to create the backbone curves of concrete. The backbone curve presents the boundary of the stress versus strain behavior for the concrete. If the specimen were cyclically loaded, unloading would fall away from the backbone curve, but loading would eventually cause a return to the backbone curve.

This chapter details the equations defining the concrete model. The plasticity model presented in Malvar et al. (1994) and improved upon in Malvar et al. (1996) was used as a starting point for the creation of the model defined in this thesis. Section 3.1 shows the three loading surfaces that underlie this model. Within this

thesis, the term *loading surface* describes a surface that is fixed in the invariant space. The loading surfaces are a tool to define the location of the *failure surface*. The failure surface defines the boundary between elastic and plastic loading, as discussed in Section 2.2. Section 3.2 defines the current failure surface, which moves between the three fixed loading surfaces. Section 3.3 discusses the final component of the concrete model, the flow rule. Section 3.4 summarizes the input parameters required to utilize the model. Section 3.5 derives the tangent modulus tensor.

3.1   Loading Surfaces

The backbone of the model is three loading surfaces corresponding to the yield, peak, and residual stress states of the concrete, following Malvar et al. (1994). The loading surfaces are three-dimensional and are fixed in the (ξ, r, θ) invariant space. For a specimen compressed in only one direction and free in the other two orthogonal directions (uniaxial compressive loading), the surfaces correspond to the yield, peak, and residual points as shown in Figure 3.1. The current failure surface travels be-
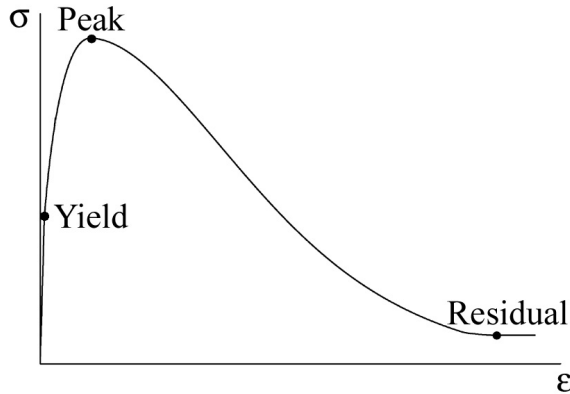
Figure 3.1: Loading surface locations.

tween these three fixed surfaces based on a damage parameter defined in Section 3.2. The equations defining the peak and residual loading surfaces are identical, while the yield loading surface is given a different shape. Values for the parameters controlling these equations are determined from experimental data for each of the three surfaces. The shape of each loading surface can be best understood by examining its shape in

two separate planes, as previously discussed in Section 2.2. The first is the meridian plane, which is the (ξ, r) plane, and represents lines of constant θ. The second is the deviatoric plane, which is the (r, θ) plane, and defines the cross section of the failure surface for constant values of ξ. By examining the behavior in these two planes, the full three-dimensional shape of the surface can be easily visualized.

The peak and residual loading surfaces are assigned a hyperbolic shape in the meridian plane as described in Section 3.1.1. This particular shape was chosen because it presented the best fit to the test data over the largest range of confinement. The shape of the test data in the meridian plane can be seen in Figures 4.3 and 4.4 for the peak surface and Figure 4.18 for the residual surface. The yield loading surface has a different shape in the meridian plane, which will be discussed in Section 3.1.1. The cross section for all three loading surfaces in the deviatoric plane is defined by an elliptic interpolation between the two meridians, as introduced by William and Warnke (1975). This is the most common approach for the deviatoric plane, as it meets all the requirements for a concrete failure surface discussed in Chapter 2. It also produces the best fit to the test data shown in Figure 4.11. Section 3.1.2 shows the equations defining this elliptic shape.

3.1.1 Meridians

The peak and residual loading surfaces are controlled by two hyperbolic meridians in the (ξ, r), or meridian, plane. They are denoted as the tensile and compressive meridians based on the value of the Lode angle for that meridian. Recall from Section 2.2 that the tensile and compressive meridians correspond to Lode angles of $0°$ and $60°$, respectively. For the peak and residual surfaces, these two meridians have a hyperbolic shape as described by Equation 3.1 and seen in Figure 3.2.

$$
\begin{aligned}
\frac{r_{t,i}}{f'_c} &= -\tfrac{1}{2}a_{3,i} + \sqrt{a_{0,i} + a_{1,i}\tfrac{\xi}{f'_c} + a_{2,i}\left(\tfrac{\xi}{f'_c}\right)^2 + \tfrac{1}{4}a_{3,i}^2} & \theta &= 0° \\
\frac{r_{c,i}}{f'_c} &= -\tfrac{1}{2}b_{3,i} + \sqrt{b_{0,i} + b_{1,i}\tfrac{\xi}{f'_c} + b_{2,i}\left(\tfrac{\xi}{f'_c}\right)^2 + \tfrac{1}{4}b_{3,i}^2} & \theta &= 60°
\end{aligned}
\qquad i = \text{peak, residual}
$$

$$(3.1)$$

The concrete compressive strength, f'_c, is defined in the accepted fashion as the compressive strength at 28 days of a uniaxially loaded cylinder, with a height equal to twice the width (ACI Committee 318, 2000). Note that values of ξ are negative for
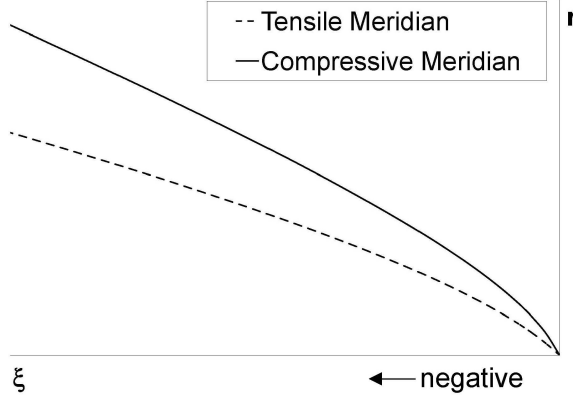
Figure 3.2: Shape of the peak and residual tensile and compressive meridians in the (ξ, r) space. Note that values of ξ are negative for compression.

compression. The invariants ξ and θ are defined in Equations 2.10 and 2.12, respectively. Values of the parameters a_0 through a_3 and b_0 through b_3 are determined from test data in Section 4.2.3 for the peak surface and Section 4.3.3 for the residual loading surface.

The yield loading surface is not based on hyperbolic meridians. It is well known that the yield point for concrete is not precisely defined due to the gradual onset of yielding. However, a single yield surface is designated at the initiation of yielding, rather than using multiple surfaces to define a yield region. The region of yielding will be accounted for through the transition of the failure surface from the yield surface to the peak surface, wherein damage is accumulating but strain softening has not yet initiated. Strain softening is defined as the region in which the stress in the material is actually decreasing with an increase in strain. The location of the yield surface is somewhat arbitrary but should be close to the initial onset of yielding. The test data show that the peak and residual stresses increase more significantly with confinement than the yield stress. Whereas the peak and residual stresses increase hyperbolically with confinement, the yield stress approaches a constant. Thus, the

following equation is chosen to define the meridians for the yield loading surface:

$$
\begin{aligned}
\frac{r_{t,yield}}{f'_c} &= -c\frac{\xi}{f'_c}\left(1 - \frac{\xi}{f'_c}\right)^{-1} & \theta &= 0° \\
\frac{r_{c,yield}}{f'_c} &= -d\frac{\xi}{f'_c}\left(1 - \frac{\xi}{f'_c}\right)^{-1} & \theta &= 60°
\end{aligned}
\tag{3.2}
$$

The shape of the yield tensile and compressive meridians is shown in Figure 3.3.
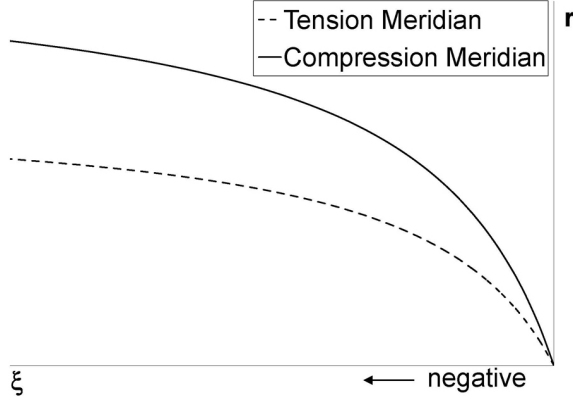
Figure 3.3: Shape of the yield tensile and compressive meridians in the (ξ, r) space. Note that values of ξ are negative for compression.

There are eighteen parameters (the a and b series for the peak and residual surfaces, and c and d for the yield surface) that control the increase in the failure deviatoric stress due to confinement. For all three loading surfaces, the difference between the a and b series of parameters (or c and d for the yield loading surface) accounts for the change in deviatoric stress caused by the Lode angle passing from 0° to 60°. It can be seen from test data that the deviatoric stress at yield, peak, or residual is lower at a Lode angle of 0° then at 60°. Thus, the tensile meridian will always have a smaller magnitude than the compressive meridian as seen in Figure 3.2. Equations 3.1 and 3.2 account for the increase in the strength of concrete as a result of confinement. The magnitude of ξ increases with increasing confinement. Through Equations 3.1 and 3.2, higher magnitudes of ξ lead to higher values for r before the failure surface is reached. The increase in the magnitudes of both ξ and r equate to larger stresses being supported by the concrete under confinement.

3.1.2 Elliptic Fit

The shape of the loading surface in the deviatoric plane is chosen as an elliptic curve, shown in Figure 3.4, defined by a method introduced in William and Warnke (1975). By using an ellipse, all the conditions of smoothness, symmetry, and convexity dis-
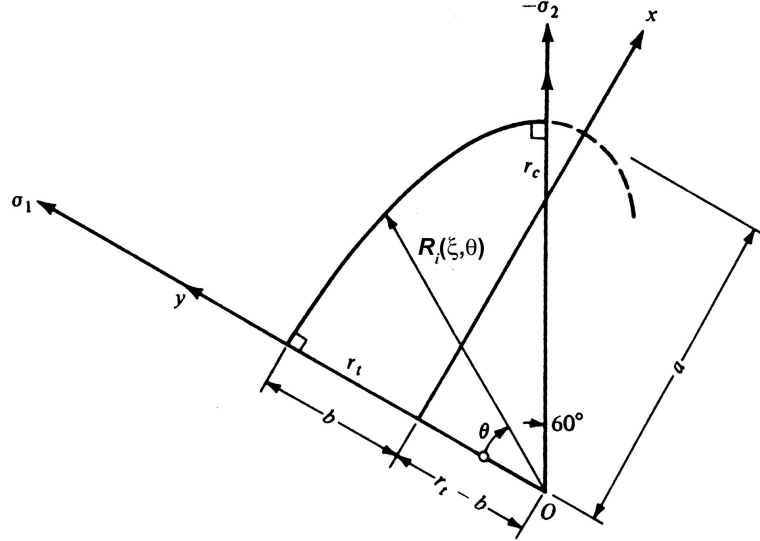
Figure 3.4: Elliptic trace of the failure surface for $0° \leq \theta \leq 60°$. Based on Chen (1982).

cussed in Chapter 2 are met. The elliptic curve between the two meridians is defined by Equation 3.3. The resulting full cross section of the loading surface in the deviatoric plane can be seen in Figure 3.5. Note that in Figure 3.5, the ξ axis is normal to the cross section plane, which is also the plane of the page, and passes through the origin.

$$R_i(\xi, \theta) = \frac{2r_{c,i}(r_{c,i}^2 - r_{t,i}^2)\cos\theta + r_{c,i}(2r_{t,i} - r_{c,i})\sqrt{4(r_{c,i}^2 - r_{t,i}^2)\cos^2\theta + 5r_{t,i}^2 - 4r_{t,i}r_{c,i}}}{4(r_{c,i}^2 - r_{t,i}^2)\cos^2\theta + (r_{c,i} - 2r_{t,i})^2}$$

(3.3)

$$i = \text{yield, peak, residual}$$

Thus, each of the three loading surfaces is defined:

$$F_i = r - R_i(\xi, \theta) = 0 \qquad i = \text{yield, peak, residual}$$

(3.4)
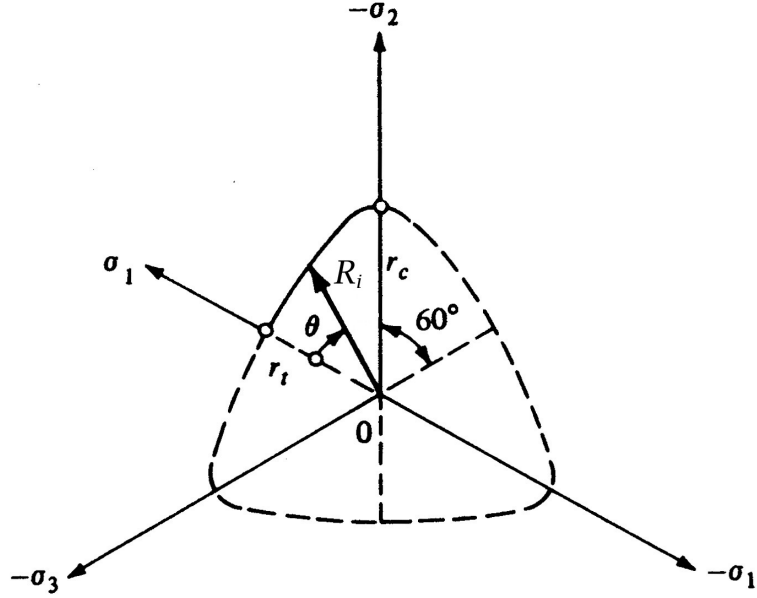
Figure 3.5: Deviatoric section of the failure surface. Modified from Chen (1982).

The invariant r is defined in Equation 2.11. The value for $R_i(\xi, \theta)$ is given by Equation 3.3 with the corresponding set of parameters for that loading surface (i.e., yield, peak, or residual).

3.2   Failure Surface

Recall that all three of these loading surfaces are fixed in the (ξ, r, θ) invariant space. The current failure surface is a linear combination of two of the three surfaces based on the current damage level, ψ. The value for ψ is integrated along the loading path of the material in order to represent the current total damage level. The incremental damage for a given load step is defined by:

$$d\psi = \frac{\overline{d\epsilon^p}}{\phi + \alpha(|\frac{\xi}{f_c'}|^\gamma)} \tag{3.5}$$

The effective plastic strain increment, $\overline{d\epsilon^p}$, was previously defined in Equation 2.17 and is restated here:

$$\overline{d\epsilon^p} = \sqrt{\frac{2}{3} d\epsilon_{ij}^p d\epsilon_{ij}^p} \tag{3.6}$$

The parameter, ϕ, defines how damage is accumulated at very low levels of stress. The invariant ξ must be located in the denominator so that large values of confinement, which result in large values for ξ, result in a decrease in the rate at which damage is accumulated. The parameters α and γ control how the damage accumulation rate is affected by confinement. Equation 3.5 is used to account for the increase in ductility seen in concrete due to increasing levels of confinement. The form of this equation is based on Malvar et al. (1994); changes were made in order to simplify the model and to better match the test data.

The location of the current failure surface based on the damage level is controlled by the variable β:

$$\beta = \left(\frac{\psi}{\psi_{peak}}\right)^{\kappa} e^{1-\left(\frac{\psi}{\psi_{peak}}\right)^{\kappa}} \tag{3.7}$$

The parameter, ψ_{peak}, defines the damage level at which the peak surface is reached. The parameter, κ, controls the rate at which the failure surface travels from one loading surface to the next. This functional form of β is based on a form derived by Smith and Young (1955) to represent the shape of the stress versus strain relationship for uniaxial compression loading shown in Figure 3.1. The value of β is zero until the load path intersects the yield loading surface. It then passes from zero to one as the current failure surface travels from the yield to the peak loading surfaces. The value of β then decreases from one back to zero as the current failure surface travels from the peak to the residual loading surface. The current failure surface can now be found by:

$$F = 0 = r - \begin{cases} \beta \left(R_{peak}(\xi,\theta) - R_{yield}(\xi,\theta)\right) + R_{yield}(\xi,\theta) & \psi \leq \psi_{peak} \\ \beta \left(R_{peak}(\xi,\theta) - R_{residual}(\xi,\theta)\right) + R_{residual}(\xi,\theta) & \psi > \psi_{peak} \end{cases} \tag{3.8}$$

The invariant r is defined in Equation 2.11. $R_{yield}(\xi,\theta)$, $R_{peak}(\xi,\theta)$, and $R_{residual}(\xi,\theta)$ are defined in Equation 3.3.

3.3 Flow Rule

Based on Malvar et al. (1996), a blend of two common flow rules was utilized which led to good agreement with test data. An associated flow rule for this model results in plastic volume expansion in excess of that indicated by test data. However, using a Prandtl-Reuss flow rule (Chen, 1982) does not allow for any plastic volume expansion, which is also not correct for concrete. Thus, a combination of the two rules is used, resulting in a nonassociated flow rule for the model.

The potential surface, Q, is therefore defined as the interpolation of two surfaces. The first surface is equal to the failure surface, as would be defined for associative flow. The second surface represents a circular cylinder passing through the failure surface at the point representing the current stress state whose axis lies along the ξ axis. This definition for Q is implemented into Equation 2.14 to determine the plastic strain increment. The parameter, ω, controls the amount of plastic volume change seen in the material. The effect of ω on the direction of plastic flow can be seen in Figure 3.6.
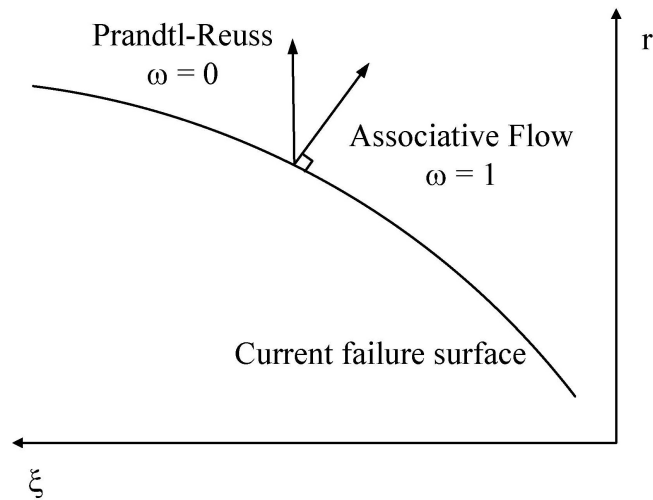
Figure 3.6: Graphical representation of the direction of plastic flow depending on ω based on Noble et al. (2005). Note that values of ξ are negative for compression.

3.4   Model Parameters

The model contains a total of twenty-four parameters that control its behavior. The values for these parameters are determined using test data in Chapter 4. A summary of these parameters and their significance is shown in Table 3.1. These twenty-four

Table 3.1: Summary of model parameters.

Name	Behavior Controlled	Total
a_0, a_1, a_2, a_3 x 2 surfaces	shape of the hyperbolic tensile meridian for the peak and residual loading surfaces	8
b_0, b_1, b_2, b_3 x 2 surfaces	shape of the hyperbolic compressive meridian for the peak and residual loading surfaces	8
c	shape of the tensile meridian for the yield loading surface	1
d	shape of the compressive meridian for the yield loading surface	1
ϕ	accumulation of damage at low stress levels	1
α, γ	accumulation of damage as a function of confinement	2
ψ_{peak}	amount of damage corresponding to the peak stress level of the concrete	1
κ	rate at which the current loading surface passes between each of the fixed surfaces	1
ω	ratio of associated plastic flow to Prandtl-Reuss plastic flow	1
Total		24

parameters can be fit to the test data for all types of concrete and defined permanently. Thus, a user of the model does not need to specially tune these parameters to the individual specimen of concrete being analyzed. However, if the user is intending to model a specific concrete mix, or a specific type of concrete, the parameters could be fit using a subset of data matching the concrete that is to be modeled. The model also requires three input parameters that are specific to the concrete specimen being modeled: the modulus of elasticity, E; Poisson's ratio, ν; and the unconfined compressive strength, f'_c, of the concrete.

3.5 Tangent Modulus Tensor

Once the plasticity model is completely defined, the consistency condition is used to derive the tangent modulus tensor, which defines the relationship between the incremental stress and strain. The consistency condition as derived in Section 2.4 and given in Equation 2.20 is:

$$dF = \frac{\partial F}{\partial \sigma_{ij}} d\sigma_{ij} + \frac{\partial F}{\partial \overline{\epsilon^p}} d\overline{\epsilon^p} = 0 \tag{3.9}$$

where $d\overline{\epsilon^p}$ is given by Equation 3.6 and the elastic stress increment, $d\sigma_{ij}$, is given by:

$$d\sigma_{ij} = D^e_{ijkl} \left(d\epsilon_{kl} - d\epsilon^p_{kl} \right) \tag{3.10}$$

D^e_{ijkl} is the elastic modulus tensor, $d\epsilon_{kl}$ the total strain increment, and $d\epsilon^p_{kl}$ the plastic strain increment as defined in Section 2.3. The definition of the plastic strain increment, as given in Equation 2.14, is restated here:

$$d\epsilon^p_{ij} = d\lambda \frac{\partial Q}{\partial \sigma_{ij}} \tag{3.11}$$

where Q is defined as discussed in Section 3.3. Substituting Equations 3.10 and 3.11 into Equation 3.9, combined with Equation 3.6 for $d\overline{\epsilon^p}$, yields an equation that can be solved for $d\lambda$:

$$d\lambda = \frac{\frac{\partial F}{\partial \sigma_{ij}} D^e_{ijkl} d\epsilon_{kl}}{\frac{\partial F}{\partial \sigma_{mn}} D^e_{mnpq} \frac{\partial Q}{\partial \sigma_{pq}} - \frac{\partial F}{\partial \overline{\epsilon^p}} \sqrt{\frac{2}{3} \frac{\partial Q}{\partial \sigma_{ij}} \frac{\partial Q}{\partial \sigma_{ij}}}} \tag{3.12}$$

Using Equation 3.12 for $d\lambda$ with Equation 3.11 yields an expression for $d\epsilon^p_{ij}$ which can be combined with Equation 3.10 to define the tangent modulus tensor.

$$d\sigma_{ij} = D^{tangent}_{ijkl} d\epsilon_{kl} = \left(D^e_{ijkl} + D^p_{ijkl} \right) d\epsilon_{kl} \tag{3.13}$$

where the plastic modulus tensor is given by:

$$D_{ijkl}^{p} = -\frac{D_{ijtu}^{e}\left(\frac{\partial Q}{\partial \sigma_{tu}}\right)\left(\frac{\partial F}{\partial \sigma_{rs}}\right)D_{rskl}^{e}}{\frac{\partial F}{\partial \sigma_{mn}}D_{mnpq}^{e}\frac{\partial Q}{\partial \sigma_{pq}} - \frac{\partial F}{\partial \bar{\epsilon}^{p}}\sqrt{\frac{2}{3}\frac{\partial Q}{\partial \sigma_{ij}}\frac{\partial Q}{\partial \sigma_{ij}}}} \tag{3.14}$$

A detailed derivation of this equation can be found in Section 8.5 of Chen (1982). Expressions for the partial derivatives in Equation 3.14 can be derived from the equations found in this chapter and are given in Appendix A. The tangent modulus tensor will be implemented into finite element code in order to utilize the material model for predicting the behavior of concrete.